Quantum squeezing schemes for heterodyne readout

Teng Zhang[*], Denis Martynov,[†] Andreas Freise[‡] and Haixing Miao[§]

School of Physics and Astronomy, and Institute of Gravitational Wave Astronomy,
University of Birmingham, Edgbaston, Birmingham B15 2TT, United Kingdom

Advanced gravitational-wave detectors are limited by quantum noise in their most sensitive frequency band. Quantum noise suppression techniques, such as the application of the quantum squeezed state of light, have been actively studied in the context of homodyne readouts. In this paper, we consider quantum squeezing schemes for the heterodyne readouts. This is motivated by a successful suppression of the higher-order-mode content by stable recycling cavities in advanced detectors. The heterodyne readout scheme requires precise tuning of the interferometer parameters and a broadband squeezing source, but is conceptually simple and elegant. We further show that it is compatible with the frequency-dependent squeezing, which reduces both the shot noise and the radiation-pressure noise. We propose a test of the heterodyne readout with squeezing in Advanced LIGO. This can serve as a pathfinder not only for the implementation in future detectors, such as the Einstein Telescope and Cosmic Explorer, but also for general high-precision optical measurements.

I. INTRODUCTION

The Pound-Drever-Hall heterodyne technique [1–9] is a powerful tool for stabilization of optical cavities in modern precision instruments, such as frequency references for optical atomic clocks, passive laser gyroscopes, and gravitational-wave detectors. In the heterodyne readout, phase modulated light probes the motion of the optical cavity and produces the signal on photodetectors at radio frequencies (rf). After demodulation, the residual signal is proportional to the cavity motion or the laser frequency noise. The heterodyne technique circumvents laser technical noise by upconverting the signal detection to frequencies where the laser light is shot-noise-limited (a few MHz) [10] but couples technical noises of the modulation oscillator [11]. In this paper, we do not focus on the technical noises of the heterodyne readout scheme and only consider the fundamental quantum noise.

Quantum noise in the heterodyne readout techniques has been previously studied in Refs. [12,13] in the context of gravitational-wave detectors. As it turns out, there are additional vacuum noises at twice the rf modulation frequency $2\omega_m$ away from the carrier frequency ω_0, which leads to 50% higher shot noise compared to the homodyne readout. The squeezed state of light can be used to suppress this additional noise, and in general, we need to have squeezing near the carrier frequency ω_0 and the two rf

sidebands frequencies $\omega_0 \pm 2\omega_m$ [9,14,15]. In this paper, we further advance these studies and consider application of quantum noise suppression techniques to the heterodyne readout in advanced gravitational-wave detectors; *i.e.*, a single squeezer is not only sufficient to improve the shot noise [16] but also can be made compatible with frequency-dependent squeezing, which reduces the quantum radiation-pressure noise. As discussed in Secs. II and III, we find that quantum squeezing works for the heterodyne readout if (i) the source of squeezed states of light has a bandwidth at least twice the rf modulation frequency (ω_m), (ii) the filter cavity for the frequency-dependent squeezing is tuned the same as in the current homodyne readout scheme, and (iii) the power imbalance of the upper and lower rf sidebands, which are on phase quadrature, is less than 10% for 12 dB broadband squeezing.

The main advantage of the homodyne readout scheme is that its quantum shot noise is a factor of $\sqrt{1.5}$ smaller compared to the one in the heterodyne readout for the same level of squeezing and optical losses. The price paid for this improvement is complexity involved in the balanced homodyne readout scheme, which requires an additional local oscillator field and optical cavities to filter the carrier field from the rf sidebands [17–20]. In Advanced LIGO, an additional local oscillator field is derived by offsetting the interferometer from its operating point. This scheme, known as dc readout [5,21–23], is also the current readout scheme in Advanced Virgo [7], KAGRA [24], and GEO 600 [21]. It has been very successful and allowed direct observation of gravitational waves for the first time [25–27]. However, the offset couples technical noise

[*]tzhang@star.sr.bham.ac.uk
[†]dmartynov@star.sr.bham.ac.uk
[‡]adf@star.sr.bham.ac.uk
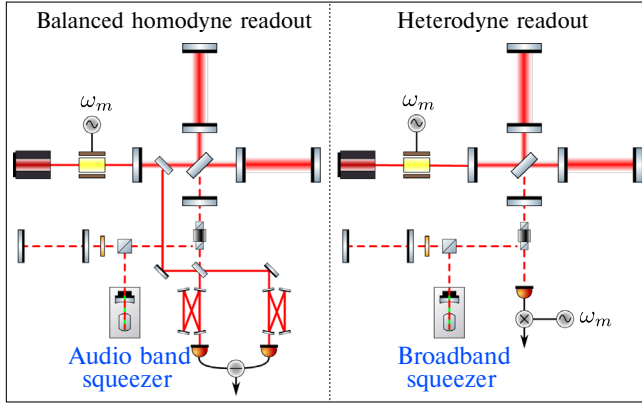[§]haixing@star.sr.bham.ac.uk

FIG. 1. Schematics of the balanced homodyne readout and the heterodyne readout, which requires a broadband squeezer with bandwidth at least twice the modulation frequency ω_m.
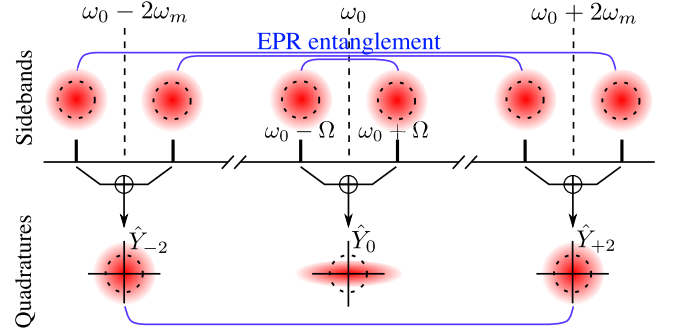

FIG. 2. Schematics of a broadband squeezer in the sideband and the quadrature picture. In contrast for an audio band squeezer, the sidebands are entangled only for Ω up to kHz.

sources and will not allow future gravitational-wave detectors to reach their design sensitivity at low frequencies [28].

The heterodyne technique is ideal for coupled optical resonators and is already used in the Advanced LIGO detectors to stabilize auxiliary degrees of freedom and for initial stabilization of the gravitational-wave channel. In this paper, we explore optical parameters when quantum noise in heterodyne and homodyne readout schemes are identical but heterodyne readout is conceptually simpler as shown in Fig. 1. This study is motivated by successful operation of the stable recycling cavities [29] in the Advanced LIGO detectors, which has significantly suppressed higher-order-mode (HOM) content in the rf sidebands due to misalignments in the cavity [30] and is also good for suppressing the HOM content from contrast defect. In Sec. IV, we show quantum noise of the Advanced LIGO detectors with the heterodyne readout and discuss steps for further improvements.

II. SQUEEZING FOR HETERODYNE READOUT

In this section, we will show the resulting quantum noise level for the heterodyne readout with a broadband squeezing. We choose the demodulation phase such that the photocurrent is proportional to the phase quadrature $\hat{Y}$, which is given by

$$\hat{Y}(\Omega) = \hat{Y}_0(\Omega) + \frac{\hat{Y}_{+2}(\Omega) + \xi\hat{Y}_{-2}(\Omega)}{1 + \xi}, \qquad (1)$$

where ξ denotes the amplitude ratio of two rf sidebands, which are on phase quadrature (more details are presented in Appendix A). Here, $\hat{Y}_0$ and $\hat{Y}_{\pm2}$ represent the phase quadrature of three modes around the carrier frequency ω_0 and the rf sidebands frequencies $\omega_0 \pm 2\omega_m$, which are linear combinations of their audio sidebands, as illustrated in Fig. 2. The last two terms contribute to the additional noise of the heterodyne

readout compared to the homodyne readout. The quantum noise level is quantified by the single-sided spectral density, which is defined for any operators $\hat{A}(\Omega)$ and $\hat{B}(\Omega')$: $\langle\psi|[\hat{A}\hat{B}^\dagger + \hat{B}^\dagger\hat{A}]/2|\psi\rangle \equiv \pi S_{AB}(\Omega)\delta(\Omega - \Omega')$. In the absence of squeezing, the quantum state $|\psi\rangle$ is in the vacuum state $|0\rangle$. Using the fact that $\langle0|[\hat{Y}_i(\Omega)\hat{Y}_j^\dagger(\Omega') + \hat{Y}_j^\dagger(\Omega')\hat{Y}_i(\Omega)]/2|0\rangle = \pi\delta(\Omega - \Omega')\delta_{ij}$ $(i, j = 0, \pm2)$, we have

$$S_{YY} = 1 + \frac{1 + \xi^2}{(1 + \xi)^2}. \qquad (2)$$

Considering the balanced case with $\xi = 1$,

$$S_{YY}|_{\text{balanced}} = \frac{3}{2}, \qquad (3)$$

which is 50% higher than that of the homodyne readout.

A. Audio band versus broadband squeezing

With the introduction of squeezing, the quantum noise level will be different, depending on the squeezing bandwidth. For the audio band squeezing, the squeezing is limited to the audio frequencies. The audio sidebands around the carrier frequency are entangled, which can be mapped to the (anti)squeezing of the corresponding amplitude quadrature $\hat{X}_0$ and the phase quadrature $\hat{Y}_0$ [31]. For the phase squeezing, the spectral densities of the quadratures satisfy the following covariance matrix:

$$\mathbb{V}_o = \begin{bmatrix} e^{2r_0} & 0 \\ 0 & e^{-2r_0} \end{bmatrix}, \qquad (4)$$

where r_0 is the squeezing factor at the audio frequencies. However, the sidebands around frequencies $\omega_o \pm 2\omega_m$ are still in the vacuum state and are uncorrelated. Therefore, the audio band squeezing results in the spectral density for $\hat{Y}$,

$$S_{YY} = e^{-2r_0} + \frac{1+\xi^2}{(1+\xi)^2}. \tag{5}$$

In contrast, as illustrated in Fig. 2, for the broadband squeezing with a bandwidth up to rf, the sidebands around frequencies $\omega_0 + 2\omega_m$ and $\omega_0 - 2\omega_m$ are entangled. Their corresponding quadratures also form the Einstein-Podolsky-Rosen (EPR) entanglement [16,31–34], and for the phase squeezing, their spectral densities satisfy the following 4×4 covariance matrix:

$$\mathbb{V}_{\pm} = \begin{bmatrix} \alpha & 0 & \beta & 0 \\ 0 & \alpha & 0 & -\beta \\ \beta & 0 & \alpha & 0 \\ 0 & -\beta & 0 & \alpha \end{bmatrix}, \tag{6}$$

where $\alpha = \cosh 2r_{2\omega_m}$, $\beta = \sinh 2r_{2\omega_m}$ with $r_{2\omega_m}$ denoting the squeezing factor at twice of the rf. As we can see, the uncertainties of the individual quadratures are larger than that of the vacuum, namely $S_{Y_{+2}Y_{+2}} = S_{Y_{-2}Y_{-2}} = \alpha \geq 1$. However, the sum of their phase quadratures, $\hat{Y}_s = (\hat{Y}_{+2} + \hat{Y}_{-2})/\sqrt{2}$, has uncertainty less than 1, namely, $S_{Y_sY_s} = \alpha - \beta = e^{-2r_{2\omega_m}}$. With a broadband squeezer, the spectral density for Y reads

$$S_{YY} = \frac{3}{2}e^{-2r} + \left(\frac{1-\xi}{1+\xi}\right)^2 \frac{e^{2r}}{2}, \tag{7}$$

where we have assumed $r_0 = r_{2\omega_m} \equiv r$ for simplicity. If two rf sidebands were balanced with $\xi = 1$,

$$S_{YY}|_{\text{balanced}} = \frac{3}{2}e^{-2r}. \tag{8}$$

The additional noise due to the fluctuations around $\omega_0 \pm 2\omega_m$ is smaller by a factor of e^{2r} comparing with Eq. (3). Figure 3 shows S_{YY} as a function of the sidebands imbalance. With 10% imbalance in the sideband power, i.e., $\xi = \sqrt{0.9}$, there is still around 10 dB quantum noise suppression for 12 dB input broadband squeezing.

B. Frequency-dependent squeezing

Frequency-dependent squeezing has been proposed to simultaneously suppress the shot noise and the quantum radiation-pressure noise in gravitational-wave detectors [35]. It uses a Fabry-Perot cavity as the filter cavity to transform the squeezed light and will be implemented in, e.g., the Advanced LIGO plus upgrade. In this section, we will show the suppression of the additional noise with the broadband squeezing also holds for the frequency-dependent squeezing.

The filter cavity imprints different phases on the sidebands, which effectively creates a frequency-dependent
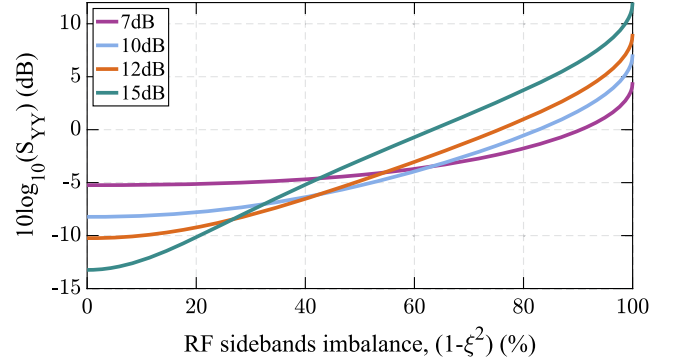

FIG. 3. Quantum noise level in dB for the heterodyne readout as a function of the power imbalance of two rf sidebands, considering different broadband squeezing lever.

rotation of the quadratures. Mathematically, the rotation is described by the following transfer matrix [36]:

$$R = e^{i\Phi} \begin{bmatrix} \cos\theta & -\sin\theta \\ \sin\theta & \cos\theta \end{bmatrix}. \tag{9}$$

Here, the phase Φ and rotation angle θ are

$$\Phi = \text{atan}\frac{2\gamma\Omega}{\gamma^2 + \Delta^2 - \Omega^2}, \quad \theta = \text{atan}\frac{2\gamma\Delta}{\gamma^2 - \Delta^2 + \Omega^2}. \tag{10}$$

The frequency γ is the filter cavity bandwidth. The frequency Δ is the cavity detuning and is different for the three modes: $\Delta \equiv \Delta_0$ for the mode around the carrier frequency; for rf modes around $\omega_0 \pm 2\omega_m$,

$$\Delta_{\pm 2} \equiv \Delta_0 \pm \text{mod}(2\omega_m, \text{FSR}), \tag{11}$$

where FSR is the free spectral range of the filter cavity.

In the balanced case, the spectral density of the additional noise due to fluctuations around $\omega_0 \pm 2\omega_m$ is

$$S_{YY}^{\text{add}} = \frac{1}{2}[\alpha - \beta\cos(\Phi_{+2} - \Phi_{-2})\cos(\theta_{+2} + \theta_{-2})], \tag{12}$$

where $\Phi_{\pm 2}$ and $\theta_{\pm 2}$ are the phase and rotation angle for quadratures of $\omega_0 \pm 2\omega_m$. Ideally, we want $\Phi_{\pm 2} = \theta_{\pm 2} = 0$, so that $S_{YY}^{\text{add}} = (\alpha - \beta)/2 = e^{-2r_{2\omega_m}}/2$, which leads to the minimum additional noise. This can be approximately achieved when $\Delta_{\pm 2}$ is much larger than the filter cavity bandwidth γ, namely having $2\omega_m$ away from any FSR of the filter cavity. As an illustration, in Fig. 4, we show the additional noise as a function of the distance of $2\omega_m$ away from the FSR (normalized by γ). We assume a filter cavity parameter the same as the A + design, namely, the cavity bandwidth $\gamma/(2\pi) = \Delta_0/(2\pi) = 45.8$ Hz. Indeed, when $2\omega_m$ is offset from $N \times$ FSR by 200 times of the filter cavity bandwidth, the additional noise level is close to
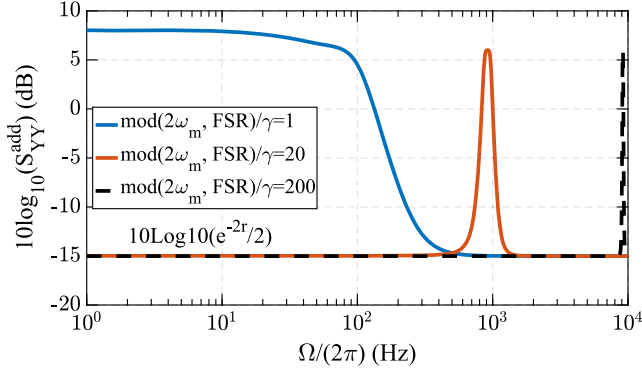
FIG. 4.   Plot shows the level of the additional noise from $\omega_0 \pm 2\omega_m$ in the phase quadrature at the reflection port of the filter cavity for different rf ω_m. The broadband squeezing level is assumed to be 12 dB. The optical parameters of the filter cavity are the same as A + design.

$e^{-2r_{2\omega_m}}/2$ for the entire frequency band relevant to gravitational-wave signals. Here N is an arbitrary integer.

III. HIGHER-ORDER-MODES AND SCHNUPP ASYMMETRY

In comparison with the homodyne readout, there are two new quantum-noise related issues associated with the heterodyne readout. The first issue is the higher-order-mode content leaking through the dark port due to the absence of output mode cleaner, which shall be traded off with the benefit of removing the output mode cleaner that induces the mode mismatch and misalignment loss. The second issue has to do with vacuum fluctuations around $\omega_0 \pm 2\omega_m$, which transmit from the bright port to the dark port due to the Schnupp asymmetry. They act like additional optical losses.

In the absence of output mode cleaner, the high-order-mode content at the carrier frequency and in the rf sidebands will both introduce additional quantum noise at $\omega_0 \pm \omega_m$, which are in the vacuum sate. We define the ratio of the power of the higher-order-mode content to the total sideband power as $\zeta_{\text{HOM}} = \zeta^0_{\text{HOM}} + \zeta^{\omega_m}_{\text{HOM}}$, in which ζ^0_{HOM} represents carrier frequency components and $\zeta^{\omega_m}_{\text{HOM}}$ represents rf components. In the case of balanced rf sidebands, the total quantum noise spectral density of the heterodyne readout is

$$S^{\text{Heterodyne}}_{YY} = \frac{3}{2}e^{-2r} + \zeta^0_{\text{HOM}} + m\zeta^{\omega_m}_{\text{HOM}}, \qquad (13)$$

where m is between 1 and 1.5 depending on the mode coherence between upper and lower rf sideband. For the homodyne readout, the output mode cleaner loss, quantified by ζ_{OMC}, also leads to a degradation of the squeezing, namely,

$$S^{\text{Homodyne}}_{YY} = (1 - \zeta_{\text{OMC}})e^{-2r} + \zeta_{\text{OMC}}. \qquad (14)$$
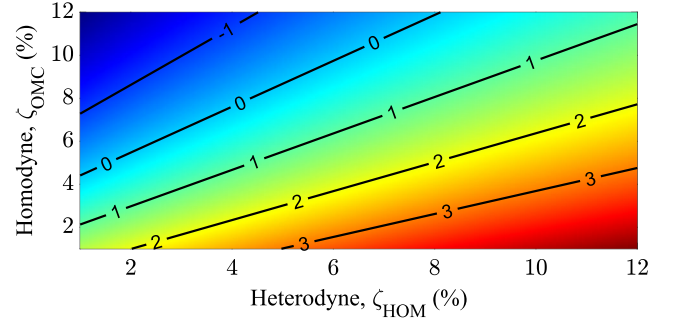

FIG. 5.   Figure shows the ratio of the quantum noise spectral density of the heterodyne readout over the that of homodyne readout as a function of the OMC loss (ζ_{OMC}) in homodyne readout and HOM content (ζ_{HOM}) in heterodyne readout in the unit of dB. The contour line of 0 dB denotes the cases when the two noise levels are equal. 12 dB input squeezing is assumed.

In Fig. 5, we show the ratio of these two spectral densities in dB as a function of ζ_{HOM} and ζ_{OMC}. We take the lower bound shot noise contribution from HOM content in rf sidebands, *i.e.,* $m = 1$.

The Schnupp asymmetry allows the rf sidebands from the bright port to transmit to the readout port (dark port) as the local oscillator for the heterodyne readout. However, it also couples the vacuum noise from the bright port to the dark port, which is equivalent to introducing optical loss to the broadband squeezing near twice of the rf. Such a loss is determined by the transmissivity of the coupled power and signal recycling cavities, which depends on the optical properties of three components: the power recycling mirror, the signal recycling mirror, and the central Michelson. In particular, the effective amplitude transmissivity and reflectivity of the central Michelson is, according to Ref. [37], $t_{\text{MI}} = -\sin \omega_m \Delta L/c$, $r_{\text{MI}} = -\cos \omega_m \Delta L/c$, where ΔL is the Schnupp asymmetry and c is the speed of light. In advanced LIGO, the 45 MHz sidebands resonate in both power recycling cavity and signal recycling cavity. The resonance condition of 90 MHz filed is different; it still resonates in signal recycling cavity but antiresonates in power recycling cavity. The effective optical loss for 90 MHz and the transmissivity for 45 MHz are shown in the Fig. 6. As we can see, in current aLIGO configuration, the optical loss for 90 MHz squeezing fields is around 0.2%. And the transmission of 45 MHz sidebands can be adjusted significantly by tuning the Schnupp asymmetry or the signal recycling mirror transmissivity without boosting the optical loss at 90 MHz significantly.

IV. HETERODYNE IN ADVANCED LIGO

In this section, we illustrate our findings in Secs. II and III on the example of the Advanced LIGO detectors, which currently operate with squeezing and homodyne readout [38]. The source injects 7.2 ± 0.3 dB of squeezing and the maximum observed level is 3.2 ± 0.1 dB. The discrepancy
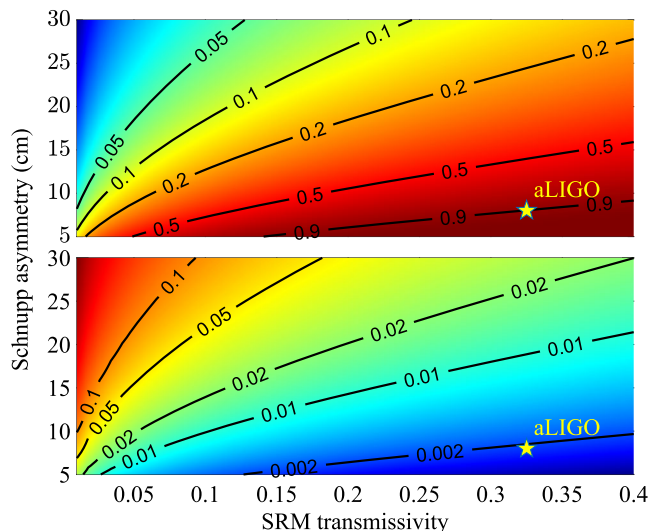
FIG. 6. The top panel shows the transmissivity for 45 MHz sidebands. The bottom panel is the equivalent optical loss for squeezing around 90 MHz as a function of the Schnupp asymmetry and the SRM transmissivity. The stars are rough estimates for the current situation of Advanced LIGO (aLIGO).

between the amount of injected and observed squeezing comes from the optical losses in the interferometer. According to Ref. [38], around 25% of the signal is lost on the Faraday isolators, on the output mode cleaner, and photodiodes. Another 10% of the signal is lost on some optical components yet to be identified.

If switched to the heterodyne readout, the quantum noise level in the Advanced LIGO detectors would be

$$S_{YY}^{\text{total}} = (1 - \epsilon_0)e^{-2r_0} + \epsilon_0$$
$$+ \frac{1}{2}[(1 - \epsilon_{2\omega_m})e^{-2r_{2\omega_m}} + \epsilon_{2\omega_m})] + \zeta_{\text{HOM}}^0 + \zeta_{\text{HOM}}^{\omega_m},$$
(15)

where ϵ_0 and $\epsilon_{2\omega_m}$ are optical losses of the interferometer near the carrier frequency and rf sidebands at $2\omega_m$, respectively. For the current Advanced LIGO configuration, according to Ref. [39], $\zeta_{\text{HOM}} = 0.12$ and the higher-order-mode content is dominated by the 02 modes of the rf sideband. The bandwidth of the LIGO squeezing source is ~10 MHz [40], which is much smaller than $2\omega_m = 90$ MHz, and therefore, we have $r_{2\omega_m} \approx 0$. Furthermore, the loss from the mode matching and alignment of the output mode cleaner which is 5%–15% in the homodyne readout scheme is negligible in the heterodyne readout, as it does not require output mode cleaner. Using the parameters discussed above and Eq. (15) we estimate the final observed squeezing is around 1.7 ± 0.2 dB for the heterdoyne readout in the current Advanced LIGO detectors.

The LIGO parameters can be optimised for the heterodyne readout as discussed in Secs. II and III. First, we need

to increase the bandwidth of the squeezing source above ~100 MHz. Achieving this milestone will make $r_{2\omega_m} = r_0$. The observed squeezing level will be increased up to 3.9 ± 0.2 dB. Finally, if we can suppress the 02 mode of the rf sidebands at the antisymmetric port, we will reduce the higher-order-mode content down to $\zeta_{\text{HOM}} = 0.02$, and the Advanced LIGO detectors will reach the observed level of squeezing equal to 4.7 ± 0.3 dB.

The corresponding shot noise amplitude spectral density is only a factor of ≈ 1.02 larger than the current shot noise in the Advanced LIGO detectors, which is much smaller compared to a factor of $\sqrt{1.5} \approx 1.22$ for the case of the same optical losses in both readouts. Moreover, higher input squeezing will further shrink the gap between the homodyne and heterodyne readout in our model since we remove the output mode cleaner for the heterodyne readout. Performing a test described in this section has a strong potential to help the Advanced LIGO detectors to estimate losses and technical noises of the output mode cleaner. The test will also demonstrate that squeezing of the quantum noise in the heterodyne readout works according to our model and can be considered for future gravitational-wave detectors.

So far, we have been focused on the cases with rf sidebands having nearly equal power. The imbalance was treated as an imperfection, which is the case for gravitational-wave detectors, as the imbalance usually introduces undesired technical noises. If the technical noises can be suppressed, we can consider more general heterdyne readouts with strongly imbalanced sidebands or even a single sideband. However, a single broadband squeezing will not be able to suppress the additional quantum noise from $\omega_0 \pm 2\omega_m$, and we would need three-mode squeezing schemes shown in Appendix B.

V. CONCLUSION AND DISCUSSION

To summarize, we have investigated squeezing schemes for the heterodyne readout in advanced gravitational-wave detectors. Our research shows that the heterodyne readout is compatible with frequency-dependent squeezing by using a broadband squeezer and a filter cavity the same as the one for the homodyne readout. We have studied the problem of the higher-order-mode content leaking to the dark port and the vacuum noise coupling from the bright port to the dark port around frequencies $\omega_0 \pm 2\omega_m$ due to the Schnupp asymmetry, which turns out to be negligible. Taking Advanced LIGO, for instance, there is a promising path to reduce the higher-order-mode content with the stable signal recycling cavity and the suppression of the dominant 02 mode. The heterodyne readout requires less auxiliary optics, and its sensitivity can be made comparable to that of the balanced homodyne readout.

The strategies of incorporating quantum squeezing into general heterodyne readout can be applied to a broad class of optical measurements that use rf sidebands as in the

Pound-Drever-Hall technique. Therefore, our findings will not only have impacts to the gravitational-wave community but also the general high-precision measurement community.

ACKNOWLEDGMENTS

APPENDIX A: DESCRIPTION OF HETERODYNE READOUT

In heterodyne readout, the rf sidebands are generated by modulating the phase of the carrier field with a rf sinusoidal signal $[m + \delta m(t)] \cos(\omega_m t + \delta \phi(t))$, where m is the modulation index, ω_m is the modulation frequency, $\delta m(t)$ is the modulation index fluctuations and $\delta \phi(t)$ is the modulation phase fluctuations. When $m \ll 1$, the laser field can be described approximately as

$$
\begin{aligned}
E(t) = & E_0 \left(1 - \frac{m^2}{4}\right) e^{i\omega_0 t} \\
& + E_0 \left[\frac{im}{2} + \frac{i\delta m(t)}{2}\right] e^{i\omega_0 t} \left(e^{-i\omega_m t} + e^{i\omega_m t}\right) \\
& + E_0 \frac{m\delta\phi(t)}{2} e^{i\omega_0 t} \left(e^{-i\omega_m t} - e^{i\omega_m t}\right) + \text{H.c.}, \quad (A1)
\end{aligned}
$$

where E_0 is the amplitude of the carrier field, H.c. denotes the Hermitian conjugate. According to Eq. (A1), we symbolize the rf local oscillator as

$$
\begin{aligned}
L(t) = & [L_+ + l_+(t)] e^{i(\omega_0 + \omega_m)t} \\
& + [L_- + l_-(t)] e^{i(\omega_0 - \omega_m)t} + \text{H.c.}, \quad (A2)
\end{aligned}
$$

where L_+, L_- are the upper and lower rf sidebands with $L_+ = L_- = i\frac{m}{2}E_0$. l_+, l_- are the fluctuation terms of the local oscillator beam. Their classical parts have the amplitude,

$$
l_+(t) = \left[\frac{i\delta m(t) - m\delta\phi(t)}{2}\right] E_0, \quad (A3a)
$$

$$
l_-(t) = \left[\frac{i\delta m(t) + m\delta\phi(t)}{2}\right] E_0. \quad (A3b)
$$

We define the signal field $Z(t)$ and specify only three modes around frequencies ω_0 and $\omega_0 \pm 2\omega_m$, which will eventually contribute to the final output. There is

$$
\begin{aligned}
Z(t) = & [\bar{Z}_0 + Z_0(t)] e^{i\omega_0 t} + Z_+(t) e^{i(\omega_0 + 2\omega_m)t} \\
& + Z_-(t) e^{i(\omega_0 - 2\omega_m)t} + \text{H.c.}, \quad (A4)
\end{aligned}
$$

where $\bar{Z}_0$ is the amplitude of the carrier that leaks to the dark port of the interferometer, $Z_0(t)$ represents the fluctuations around frequency ω_0, including both signal and noise. $Z_+(t)$ and $Z_-(t)$ represent the fluctuations around frequencies $\pm\omega_m$, respectively. Ignoring the second order terms and the terms at irrelevant frequencies, the beat between local oscillator and signal field can be calculated as

$$
\begin{aligned}
& [L(t) + Z(t)][L(t) + Z(t)]^\dagger \\
& = 2[L_+ + l_+(t)][(\bar{Z}_o + Z_o(t))^\dagger e^{i\omega_m t} + Z_+^\dagger(t) e^{-i\omega_m t}] \\
& + 2[L_- + l_-(t)][(\bar{Z}_o + Z_o(t))^\dagger e^{-i\omega_m t} + Z_-^\dagger(t) e^{i\omega_m t}] \\
& + \text{H.c.} \quad (A5)
\end{aligned}
$$

This photocurrent is then demodulated by the sinusoidal signal $[m' + \delta m'(t)] \cos(\omega_m t + \phi' + \delta\phi'(t))$, which is from the same source of modulation signal. It can be written approximately as

$$
[m' + \delta m'(t)] \cos(\omega_m t + \phi') - \delta\phi'(t) m' \sin(\omega t + \phi'), \quad (A6)
$$

where m' and $\delta m'(t)$ represent the amplitude of demodulation signal and its fluctuations; ϕ' and $\delta\phi'(t)$ represent the demodulation phase and its fluctuations. After applying a low pass filter with audio bandwidth to the product of Eqs. (A5) and (A6), we can get the demodulated output.

It is convenient to describe the output in frequency domain using quadrature operator base on the relation [13],

$$
A\hat{Z}_{-\Omega}^\dagger + A^\dagger \hat{Z}_\Omega = \sqrt{2}|A|\hat{Z}_\zeta(\Omega), \quad (A7)
$$

where $A = |A|e^{i\zeta}$ is an arbitrary complex amplitude. The quadrature operator Z_ζ is defined as

$$
Z_\zeta(\Omega) = \hat{X}(\Omega)\cos\zeta + \hat{Y}(\Omega)\sin\zeta, \quad (A8)
$$

with

$$
\hat{X}(\Omega) = \frac{\hat{Z}_\Omega + \hat{Z}_{-\Omega}^\dagger}{\sqrt{2}}, \qquad Y(\Omega) = \frac{\hat{Z}_\Omega - \hat{Z}_{-\Omega}^\dagger}{\sqrt{2}i}, \quad (A9)
$$

representing amplitude quadrature and phase quadrature, respectively. Eventually, the demodulated output can then be calculated as

$$
\begin{aligned}
I(\Omega) = & \sqrt{2}m'[|L_0|Z_{0\zeta_0}(\Omega) + |L_+|Z_{+\zeta_+}(\Omega) + |L_-|Z_{-\zeta_-}(\Omega)] \\
& + \sqrt{2}m'|\bar{Z}_0|[l_{+\alpha_+}(\Omega) + l_{-\alpha_-}(\Omega)] \\
& - 2m'\delta\phi'(\Omega)[|L_+||\bar{Z}_0|\cos\beta_+ + |L_-||\bar{Z}_0|\cos\beta_-] \\
& + 2\delta m'(\Omega)[|L_+||\bar{Z}_0|\cos\psi_+ + |L_-||\bar{Z}_0|\cos\psi_-],
\end{aligned}
$$

$$
(A10)
$$

where

$$|L_0| = |L_+ e^{-i\phi'} + L_- e^{i\phi'}|, \qquad (A11)$$

and

$$\zeta_0 = \arg\left(L_+ e^{-i\phi'} + L_- e^{i\phi'}\right), \qquad (A12a)$$

$$\zeta_\pm = \pm\phi' + \arg L_\pm, \qquad (A12b)$$

$$\alpha_\pm = \pm\phi' + \arg \bar{Z}_0, \qquad (A12c)$$

$$\beta_+ = \arg\left(L_+ e^{-i\phi'}\right) - \arg \bar{Z}_0 - \frac{\pi}{2}, \qquad (A12d)$$

$$\beta_- = \arg\left(L_- e^{i\phi'}\right) - \arg \bar{Z}_0 + \frac{\pi}{2}, \qquad (A12e)$$

$$\psi_+ = \arg\left(L_+ e^{-i\phi'}\right) - \arg \bar{Z}_0, \qquad (A12f)$$

$$\psi_- = \arg\left(L_- e^{i\phi'}\right) - \arg \bar{Z}_0. \qquad (A12g)$$

When $\bar{Z}_0 = 0$, considering balanced rf sidebands which are on phase quadrature and $\phi' = 0$ for phase measurement, there is

$$
\begin{aligned}
&I(\Omega, |L_+| = |L_-|) \\
&= \sqrt{2}m'|L_0|\left[Y_0(\Omega) + \frac{Y_{+2}(\Omega) + Y_{-2}(\Omega)}{2}\right], \quad (A13)
\end{aligned}
$$

where Y_0 and $Y_{\pm 2}$ represent the phase quadrature of three modes around frequency ω_0 and $\omega_0 \pm 2\omega_m$. If, $|L_+| \neq |L_-|$,

$$
\begin{aligned}
&I\left(\Omega, \left|\frac{|L_-|}{|L_+|}\right| = \xi\right) \\
&= \sqrt{2}(1+\xi)m'|L_+|\left[Y_0(\Omega) + \frac{Y_{+2}(\Omega) + \xi Y_{-2}(\Omega)}{1+\xi}\right],
\end{aligned}
$$
$$(A14)$$

where $\xi = \left|\frac{L_-}{L_+}\right|$ denotes the ration of amplitude of two rf sidebands on phase quadrature.

APPENDIX B: THREE MODES SQUEEZING SCHEMES

In this Appendix, we introduce squeezing schemes as shown in Fig. 7, which produce three independent squeezing modes around ω_0 and $\omega_0 \pm 2\omega_m$.

Scheme (a) uses three audio band squeezing sources which are coherently combined through two optical cavities that properly reflect and transmit the fields using their frequency selectivity. Scheme (b) uses a single cavity with three pumps interacting with the nonlinear crystal. The longitudinal mode frequency of the cavity coincide with
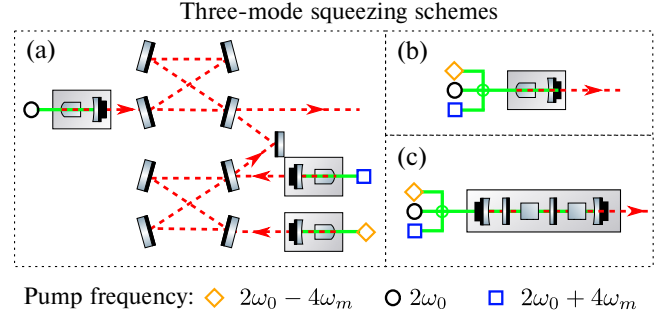
Three-mode squeezing schemes

Pump frequency: ◇ $2\omega_0 - 4\omega_m$ ○ $2\omega_0$ □ $2\omega_0 + 4\omega_m$

FIG. 7. Different three-mode squeezing schemes to produce independent squeezing fields near $\omega_0 - 2\omega_m$, ω_0, and $\omega_0 + 2\omega_m$ for general imbalanced heterodyne readouts. Scheme (a) coherently combines the squeezing from three independent sources. Scheme (b) uses three longitudinal modes of a single cavity, which are separated by the free spectral range equal to $2\omega_m$. It works when the crystal squeezing bandwidth is smaller than $2\omega_m$. Otherwise, a more sophisticated scheme (c) with three cavities coupled together can be an option.

that of three squeezing modes. The squeezing bandwidth of the crystal, however, needs to be smaller than $2\omega_m$ to avoid the EPR entanglement between neighboring modes. If it is challenging to achieve, we can consider scheme (c), which uses coupled cavities and two nonlinear crystals.

In scheme (c), we define the optical modes of the three cavities as a, b and c with identical frequency ω_E. The power transmissivities of the mirrors between cavities a, b is defined as T_1; the power transmissivities of the mirrors between cavities b, c is defined as T_2. The cavities lengths are defined as L_a, L_b, L_c. They should satisfy that the cavity coupling frequencies between each pair of adjacent cavities are identical. So the coupling frequency ω_c can be calculated as [41]

$$\omega_c = \frac{c\sqrt{T_1}}{2\sqrt{L_a L_b}} = \frac{c\sqrt{T_2}}{2\sqrt{L_b L_c}}. \qquad (B1)$$

In the interaction picture, the optical part of the Hamiltonian of the three coupled cavities can be written as

$$\mathcal{H}_{\text{opt}} = \hbar\left[a^\dagger b^\dagger c^\dagger\right]\begin{bmatrix} \omega_E & \omega_c & 0 \\ \omega_c & \omega_E & \omega_c \\ 0 & \omega_c & \omega_E \end{bmatrix}\begin{bmatrix} a \\ b \\ c \end{bmatrix}. \qquad (B2)$$

The decoupled eigenmodes of the three coupled cavities, n_0, $n_\pm$, can be derived by diagonalizing the matrix above, which gives

$$\begin{bmatrix} a \\ b \\ c \end{bmatrix} = \begin{bmatrix} \frac{1}{\sqrt{2}} & \frac{1}{2} & \frac{1}{2} \\ 0 & -\frac{1}{\sqrt{2}} & \frac{1}{\sqrt{2}} \\ -\frac{1}{\sqrt{2}} & \frac{1}{2} & \frac{1}{2} \end{bmatrix}\begin{bmatrix} n_0 \\ n_- \\ n_+ \end{bmatrix}. \qquad (B3)$$

The three eigenmodes have eigenfrequencies, ω_E and $\omega_E \pm \sqrt{2}\omega_c$. For our purpose, we need

$$\omega_c = \sqrt{2}\omega_m. \tag{B4}$$

The Hamiltonian describing the interactions in the system can be written as [42]

$$\mathcal{H}_I = -\frac{i\hbar}{2}\left[\chi_0^a \frac{n_0{}^2 + n_+ n_-}{2} + \chi_-^a \frac{n_-{}^2}{4} + \chi_+^a \frac{n_+{}^2}{4} \right.$$
$$\left. - \sqrt{2}\chi_0^b n_+ n_- + \chi_-^b \frac{n_-{}^2}{2} + \chi_+^b \frac{n_+{}^2}{2}\right] + \text{H.c.}, \tag{B5}$$

where each constant, $\chi_0^a, \chi_-^a, \chi_+^a, \chi_0^b, \chi_-^b, \chi_+^b$ is proportional to the second-order nonlinear susceptibility of crystal in cavity

a and b and the amplitude of the pumps. By designing the power of pumps and crystal features satisfying $\chi_0^a = 2\sqrt{2}\chi_0^b$, the correlations between mode n_+ and n_- can be coherently canceled. Thus, Eq. (B5) can be rewritten as

$$\mathcal{H}_I = -\frac{i\hbar}{2}\left(g_0 n_0^{\dagger 2} + g_- n_-^{\dagger\,2} + g_+ n_+^{\dagger\,2}\right) + \text{H.c.}, \tag{B6}$$

where

$$g_0 = \frac{\chi_0^a}{2}, \quad g_- = \frac{\chi_-^a + 2\chi_-^b}{4}, \quad g_+ = \frac{\chi_+^a + 2\chi_+^b}{4}. \tag{B7}$$

It is then straightforward to see the three pairs of independent interactions, which will give three modes of single mode squeezing.

[1] R. W. P. Drever, J. L. Hall, F. V. Kowalski, J. Hough, G. M. Ford, A. J. Munley, and H. Ward, Laser phase and frequency stabilization using an optical resonator, Appl. Phys. B **31**, 97 (1983).

[2] E. D. Black, An introduction to pounddreverhall laser frequency stabilization, Am. J. Phys. **69**, 79 (2001).

[3] R. Takahashi (TAMA Collaboration), Status of TAMA300, Classical Quantum Gravity **21**, S403 (2004).

[4] D. Sigg (LIGO Scientific Collaboration), Status of the LIGO detectors, Classical Quantum Gravity **25**, 114041 (2008).

[5] J. Aasi, B. P. Abbott, R. Abbott, T. Abbott, M. R. Abernathy, K. Ackley, C. Adams, T. Adams, P. Addesso, and R. X. Adhikari (LIGO Scientific Collaboration), Advanced LIGO, Classical Quantum Gravity **32**, 074001 (2015).

[6] F. Acernese et al., The status of VIRGO, Classical Quantum Gravity **23**, S63 (2006).

[7] F. Acernese et al., Advanced virgo: A second-generation interferometric gravitational wave detector, Classical Quantum Gravity **32**, 024001 (2015).

[8] K. L. Dooley and (LIGO Scientific Collaboration), Status of GEO 600, J. Phys. Conf. Ser. **610**, 012015 (2015).

[9] V. Chickarmane, S. V. Dhurandhar, T. C. Ralph, M. Gray, H.-A. Bachor, and D. E. McClelland, Squeezed light in a frontal-phase-modulated signal-recycled interferometer, Phys. Rev. A **57**, 3898 (1998).

[10] M. Rakhmanov, Demodulation of intensity and shot noise in the optical heterodyne detection of laser interferometers for gravitational waves, Appl. Opt. **40**, 6596 (2001).

[11] R. Ward, Length sensing and control of a prototype advanced interferometric gravitational wave detector, Ph.D. Thesis, Caltech, 2010.

[12] T. M. Niebauer, R. Schilling, K. Danzmann, A. Rüdiger, and W. Winkler, Nonstationary shot noise and its effect on the sensitivity of interferometers, Phys. Rev. A **43**, 5022 (1991).

[13] A. Buonanno, Y. Chen, and N. Mavalvala, Quantum noise in laser-interferometer gravitational-wave detectors with a heterodyne readout scheme, Phys. Rev. D **67**, 122005 (2003).

[14] B. J. Meers and K. A. Strain, Modulation, signal, and quantum noise in interferometers, Phys. Rev. A **44**, 4693 (1991).

[15] C. M. Caves, Quantum-mechanical noise in an interferometer, Phys. Rev. D **23**, 1693 (1981).

[16] J. Gea-Banacloche and G. Leuchs, Squeezed states for interferometric gravitational-wave detectors, J. Mod. Opt. **34**, 793 (1987).

[17] P. Fritschel, M. Evans, and V. Frolov, Balanced homodyne readout for quantum limited gravitational wave detectors, Opt. Express **22**, 4224 (2014).

[18] T. Zhang, S. L. Danilishin, S. Steinlechner, B. W. Barr, A. S. Bell, P. Dupej, C. Gräf, J.-S. Hennig, E. A. Houston, S. H. Huttner, S. S. Leavey, D. Pascucci, B. Sorazu, A. Spencer, J. Wright, K. A. Strain, and S. Hild, Effects of static and dynamic higher-order optical modes in balanced homodyne readout for future gravitational waves detectors, Phys. Rev. D **95**, 062001 (2017).

[19] S. Steinlechner, B. W. Barr, A. S. Bell, S. L. Danilishin, A. Gläfke, C. Gräf, J.-S. Hennig, E. A. Houston, S. H. Huttner, S. S. Leavey, D. Pascucci, B. Sorazu, A. Spencer, K. A. Strain, J. Wright, and S. Hild, Local-oscillator noise coupling in balanced homodyne readout for advanced gravitational wave detectors, Phys. Rev. D **92**, 072009 (2015).

[20] T. Zhang et al., Quantum noise cancellation in asymmetric speed metres with balanced homodyne readout, New J. Phys. **20**, 103040 (2018).

[21] S. Hild, H. Grote, J. Degallaix, S. Chelkowski, K. Danzmann, A. Freise, M. Hewitson, J. Hough, H. Lck, M. Prijatelj, K. A. Strain, J. R. Smith, and B. Willke, DC-readout of a signal-recycled gravitational wave detector, Classical Quantum Gravity **26**, 055012 (2009).

[22] T. T. Fricke, N. D. Smith-Lefebvre, R. Abbott, R. Adhikari, K. L. Dooley, M. Evans, P. Fritschel, V. V. Frolov, K. Kawabe, J. S. Kissel, B. J. J. Slagmolen, and S. J. Waldman,

DC readout experiment in enhanced LIGO, Classical Quantum Gravity **29,** 065005 (2012).

[23] H. Gorte (forthe LIGO Scientific Collaboration), The GEO 600 status, Classical Quantum Gravity **27,** 084003 (2010).

[24] T. Akutsu, M. Ando, K. Arai, Y. Arai, S. Araki, A. Araya (KAGRA Collaboration), Kagra: 2.5 generation interferometric gravitational wave detector, Nat. Astron. **3,** 35 (2019).

[25] B. Abbott, R. Abbott, T. Abbott, M. Abernathy, F. Acernese, K. Ackley, C. Adams, T. Adams, P. Addesso, R. Adhikari *et al.* (LIGO Scientific and Virgo Collaborations), Observation of Gravitational Waves from a Binary Black Hole Merger, Phys. Rev. Lett. **116,** 061102 (2016).

[26] B. Abbott, R. Abbott, T. Abbott, M. Abernathy, F. Acernese, K. Ackley, C. Adams, T. Adams, P. Addesso, R. Adhikari *et al.* (LIGO Scientific and Virgo Collaborations), Gw170817: Observation of Gravitational Waves from a Binary Neutron Star Inspiral, Phys. Rev. Lett. **119,** 161101 (2017).

[27] B. Abbott, R. Abbott, T. Abbott, M. Abernathy, F. Acernese, K. Ackley, C. Adams, T. Adams, P. Addesso, R. Adhikari *et al.* (LIGO Scientific and Virgo Collaborations), Gwtc-1: A Gravitational-Wave Transient Catalog of Compact Binary Mergers Observed by Ligo and Virgo during the First and Second Observing Runs, Phys. Rev. X **9,** 031040 (2019).

[28] H. Yu, D. Martynov, S. Vitale, M. Evans, D. Shoemaker, B. Barr, G. Hammond, S. Hild, J. Hough, S. Huttner, S. Rowan, B. Sorazu, L. Carbone, A. Freise, C. Mow-Lowry, K. L. Dooley, P. Fulda, H. Grote, and D. Sigg, Prospects for Detecting Gravitational Waves at 5 hz With Ground-Based Detectors, Phys. Rev. Lett. **120,** 141102 (2018).

[29] M. A. Arain and G. Mueller, Design of the advanced ligo recycling cavities, Opt. Express **16,** 10018 (2008).

[30] A. M. Gretarsson, E. D'Ambrosio, V. Frolov, B. O'Reilly, and P. K. Fritschel, Effects of mode degeneracy in the ligo livingston observatory recycling cavity, J. Opt. Soc. Am. B **24,** 2821 (2007).

[31] R. Schnabel, Squeezed states of light and their applications in laser interferometers, Phys. Rep. **684,** 1 (2017).

[32] J. Zhang, Einstein-podolsky-rosen sideband entanglement in broadband squeezed light, Phys. Rev. A **67,** 054302 (2003).

[33] Y. Ma, H. Miao, B. H. Pang, M. Evans, C. Zhao, J. Harms, R. Schnabel, and Y. Chen, Proposal for gravitational-wave detection beyond the standard quantum limit through epr entanglement, Nat. Phys. **13,** 776 (2017).

[34] S. L. Danilishin, F. Y. Khalili, and H. Miao, Advanced quantum techniques for future gravitational-wave detectors, Living Rev. Relativity **22,** 2 (2019).

[35] H. J. Kimble, Y. Levin, A. B. Matsko, K. S. Thorne, and S. P. Vyatchanin, Conversion of conventional gravitational-wave interferometers into quantum nondemolition interferometers by modifying their input and/or output optics, Phys. Rev. D **65,** 022002 (2001).

[36] S. L. Danilishin and F. Y. Khalili, Quantum measurement theory in gravitational-wave detectors, Living Rev. Relativity **15,** 5 (2012).

[37] K. Izumi and D. Sigg, Advanced LIGO: Length sensing and control in a dual recycled interferometric gravitational wave antenna, Classical Quantum Gravity **34,** 015001 (2016).

[38] M. Tse, H. Yu, N. Kijbunchoo, A. Fernandez-Galiana, P. Dupej, and L. E. A. Barsotti, Quantum-Enhanced Advanced Ligo Detectors in the Era of Gravitational-Wave Astronomy, Phys. Rev. Lett. **123,** 231107 (2019).

[39] K. Araj, Advanced Ligo Livingston Logbook Report No. 25070, 2016.

[40] E. Oelker, Squeezed states for advanced gravitational wave detectors, Ph.D. thesis, MIT, 2016.

[41] P. Purdue and Y. Chen, Practical speed meter designs for quantum nondemolition gravitational-wave interferometers, Phys. Rev. D **66,** 122004 (2002).

[42] D. F. Walls and G. J. Milburn, *Quantum Optics* (Springer Science & Business Media, New York, 2007).